Engineering interfacial energy profile by changing the substrate terminating plane in perovskite heterointerfaces

S. Roy, A. Solmaz, J. D. Burton, M. Huijben, G. Rijnders, E. Y. Tsymbal, and T. Banerjee

Phys. Rev. B **93**, 115101 — Published 1 March 2016

DOI: 10.1103/PhysRevB.93.115101

Engineering interfacial energy profile by changing the substrate terminating plane in perovskite heterointerfaces

S. Roy,[1] A. Solmaz,[2] J. D. Burton,[3] M. Huijben,[2] G. Rijnders,[2] E. Y. Tsymbal,[3] and T. Banerjee[1,*]

[1] *Physics of Nanodevices, Zernike Institute for Advanced Materials, University of Groningen, Nijenborgh 4, 9747 AG Groningen, The Netherlands*
[2] *MESA+ Institute for Nanotechnology, University of Twente, The Netherlands*
[3] *Department of Physics and Astronomy, University of Nebraska-Lincoln, USA*

(Dated: February 10, 2016)

Atomically engineered oxide heterointerfaces show a range of novel phenomena not present in their bulk form, thus providing an additional knob to tune the functional properties across such interfaces. Here we show that for an oxide Schottky interface between metallic $SrRuO_3$ and semiconducting Nb doped $SrTiO_3$ (Nb:STO), the terminating surface of the substrate plays a crucial role in determining the electronic transport across it. Interestingly this is achieved by engineering a monolayer of charge neutral SrO layer across the Schottky interface and not by the insertion of charged layers at the interface, as has been demonstrated earlier. These changes in the energy band line-up across a symmetric interface indicate the presence of different polar characters at the SrO and TiO_2 terminations of the substrate. Owing to the presence of the same AO layer (SrO) in both $SrRuO_3$ and Nb:STO, we propose an intermixing of Ru and Ti ions across the interface for the SrO terminated Nb:STO substrate. First-principles density functional theory calculations on these systems conform with our experimental findings, and indicate a resultant shift in the interfacial atomic plane stacking of $SrRuO_3$ at the intermixed interface, leading to a modification of the electrostatic potential at the interface. The interdependence between the interfacial band alignment to the local atomic plane displacement across an intrinsically non-polar oxide heterointerface is a new mechanism in realizing novel electronic properties in oxide based devices.

PACS numbers: 73.40.-c, 73.30.y, 73.50.-h, 73.61.-r, 72.20.Ht, 73.50.Fq, 68.47.Gh

Keywords: Complex oxides, Thin films, Non-polar interfaces, Energy band-lineups, Atomic-plane displacement

I. INTRODUCTION

Interfaces between complex oxides is a rich playground where owing to the breaking of symmetry, emerging interfacial physical properties like electrical conduction[1], magnetism[2] and superconductivity[3] are exhibited. Consequently, it has led to an immense research interest in these material systems, where the major focus has been on the design and manipulation of interfaces for diverse functionalities[4]. The creation, engineering and characterization of such functional interfaces have been boosted by the evolution of sophisticated thin film techniques allowing the growth of atomically flat, lattice matched interfaces and probing them for their structure and electronic transport[5–12]. Many unique electronic phenomena like electric field control of spin lifetimes, superconductivity, metal-insulator transition and ferroelectricity have established atomic scale control of heterointerfaces as a tool to tailor their properties[1,13–23]. The ionic nature of bonding across the heterointerface precludes such oxide device properties, and the corresponding energy band alignment is dictated by the local electrostatic envioronment[24]. Atomic scale control of the ionic layer sequence in such heterointerfaces can influence the energy band alignment significantly[25,26]. For example, the introduction of an artificial interfacial dipolar layer as $(LaO)^+$ or $(AlO2)^-$ between a heterointerface of $SrRuO_3$/Nb:$SrTiO_3$ (Nb:STO) was found to lead to a modulation of the energy band alignment at the interface[27]. In this work we demonstrate that for similar metal-semiconductor (M-S) heterointerface of $SrRuO_3$/Nb:STO, we can tune the Schottky barrier height (SBH) and thus the band alignment, by inserting an interfacial layer that is charge neutral.

We have performed recent experiments on ultra-thin films of $SrRuO_3$ grown on Nb:STO substrates that demonstrate the crucial role of the film/substrate interface in the evolution of magnetism with increasing thicknesses of $SrRuO_3$[28]. Across such a similar interface, we have shown the evolution of electronic transport for different thickness of the $SrRuO_3$ film, as revealed by the differences in the electronic landscape and SBH. This provided critical insights into energy band alignments of the buried interface[29]. To establish its origin and to understand the underlying relation between structure and electronic transport at such an interface, here we engineer the surface terminating plane in $SrTiO_3$ from TiO_2 to SrO and studied its effect on tuning the interfacial band alignment. We do this by inserting a monolayer of SrO before depositing the $SrRuO_3$ layer on Nb:STO. We find that such interface engineering leads to a clear difference in the potential landscape, as manifested in the SBH extracted at both the interfaces (TiO_2 and SrO). This change arises due to different electrostatic potentials for the two interfaces, and we propose the origin as cationic intermixing of Ru and

Ti for the SrO terminated Nb:STO substrate. First principles density functional theory (DFT) calculations on these interfaces conform to our experimental findings.

This study involves two different types of devices, viz. devices with TiO_2 termination of the Nb:STO substrate (T-Nb:STO) and devices with a monolayer of SrO on a TiO_2 terminated substrate (S-Nb:STO). For T-Nb:STO, few local regions with SrO termination also can occur along terrace edges on the terminated surface[30]. Electronic transport across the buried interface for both devices (T-Nb:STO/S-Nb:STO) were probed with a nanoscale transport technique namely ballistic electron emission microscopy (BEEM). SBHs were extracted for both types of devices and it was found that the local SBH extracted for $SrRuO_3$ grown on S-Nb:STO and on local SrO terminations of T-Nb:STO were alike, and that it was consistently higher than for $SrRuO_3$ grown on T-Nb:STO devices. We also present a comparative study of the atomic structure at the film-substrate interfaces for both devices as obtained from our DFT calculations. Interatomic plane displacements for the two interfaces clearly illustrate different displacements of the SrO atomic planes of $SrRuO_3$ for S-Nb:STO and T-Nb:STO. These observations are strongly correlated to the electronic properties of both interfaces, as reflected in our transport studies and the DFT results strongly corroborate our experimental findings. Such functionalities across these interfaces have not been reported earlier.

II. EXPERIMENTAL

Thin films of $SrRuO_3$ were grown by pulsed laser deposition (PLD) on Nb-doped (0.01 wt %) $SrTiO_3$ (001) substrates while the surface quality was monitored by reflective high-energy electron diffraction (RHEED). A combined chemical and thermal treatment was applied to achieve a single TiO_2 termination of the Nb:STO substrates[31]. However, no chemical treatments have been reported to produce the opposite single-terminated SrO surfaces, while heat treatment of the as-received $SrTiO_3$ substrates usually results in a mixed termination. The single-terminated SrO surfaces can be obtained by deposition of a SrO monolayer on a single-terminated TiO_2 surface. For epitaxial SrO monolayer growth, pulsed laser interval deposition was applied[32]. In this deposition technique, the total number of laser pulses for one monolayer has to be provided rapidly (50 Hz) to stabilize the correct SrO layer without multilevel islands. Concerning the deposition conditions, a single-crystal SrO target is ablated with an energy density of 1.3 J/cm^2. During growth, the substrate is held at 850°C in an oxygen environment at 0.13 mbar. This results in crystalline SrO-terminated $SrTiO_3$ surfaces with perfectly straight step edges[33].

Subsequently, $SrRuO_3$ thin films of 8 unit cells (u.c.) were deposited on both types of single-terminated Nb:STO substrates. The growth was carried out on a substrate kept at 600°C in an oxygen environment at 0.13 mbar. Figures 1(a) and 1(b) show the RHEED specular spot intensity during the deposition of $SrRuO_3$ on T-Nb:STO and for the growth of one monolayer of SrO followed by 8 u.c. of $SrRuO_3$ respectively. The oscillations of the RHEED intensity indicates a partially layer-by-layer growth mode in both cases. The corresponding RHEED diffraction images clearly show sharp two dimensional spots, indicating diffraction from smooth crystalline surfaces. Figure 1(c) shows the atomic force microscopy (AFM) images of the 8 u.c. $SrRuO_3$ grown on both types of single-terminated surfaces (T-Nb:STO/S-Nb:STO). The low level of surface roughness was confirmed for both cases as the micrographs and roughness analyses show smooth terraces with unit cell steps. However, for $SrRuO_3$ films grown on T-Nb:STO small regions can be observed with the formation of narrow trenches at the step edges. This formation was previously reported to result from the coexistence of TiO_2 as well as SrO termination leading to disparate growth kinetics of the deposited $SrRuO_3$ thin film[30]. The presence of both terminations with well-defined lateral separation in a single T-Nb:STO sample enables us to study the local difference in transport behavior and compare it to the S-Nb:STO sample with full SrO termination.

The as-grown films were then patterned into devices using UV lithography and Ion Beam etching (IBE). Figure 2(a) shows the measurement scheme including the design of the sample being measured. An Ohmic back contact was realized by evaporating Ti/Au over a large area, which acts as the collector in this transport geometry. The devices were transferred into an ultra-high vacuum (UHV) scanning tunneling microscopy (STM)/BEEM system for measurement. The measurements were conducted at room temperature (300 K). BEEM is a three terminal modification of an STM which is used to study carrier transport through the buried M-S interface, at different energies, with high spatial resolution[34–37]. The tip of an STM is used as an emitter and is set to a bias $-V_T$ resulting in the injection of a distribution of hot electrons into the $SrRuO_3$ metal base. Upon injection, they undergo scattering and a few hot electrons, after transmission through the $SrRuO_3$ film are collected in the conduction band (CB) of Nb:STO. The Schottky barrier(ϕ) at the M-S interface acts as an energy filter, allowing only those electrons to pass through that have enough energy to overcome the barrier. In other words, while doing spectroscopy studies no BEEM current (I_B) is observed for a voltage below a threshold value when the electrons do not possess enough energy to overcome the Schottky barrier(ϕ) at the M-S interface. Additionally, by moving the tip across different areas of the device, information on spatial homogeneity of ϕ can be obtained. The energy

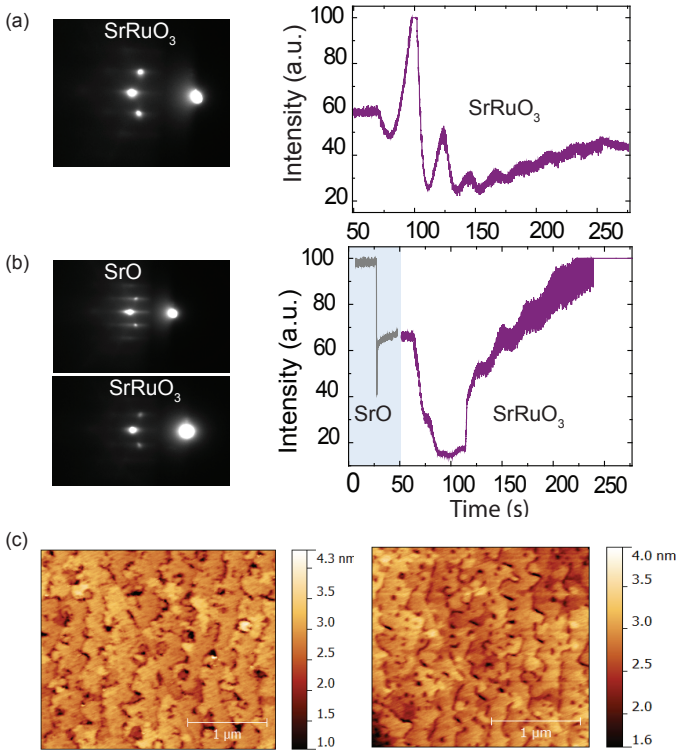

FIG. 1. Growth of 8 u.c. of $SrRuO_3$ on TiO_2 and SrO terminated substrates. (a) RHEED data for $SrRuO_3$ growth on non-engineered substrate T-Nb:STO. (b) RHEED data for the growth of a monolayer of SrO followed by 8 u.c. of $SrRuO_3$. (c) AFM scan image of T-Nb:STO and S-Nb:STO.

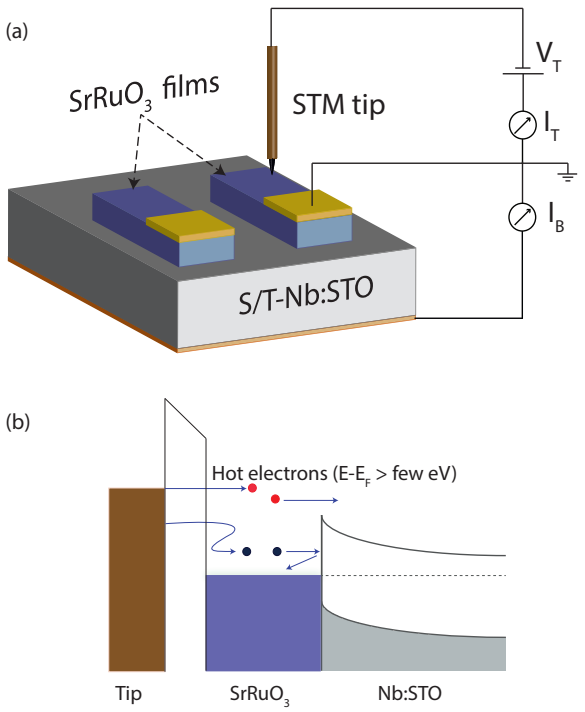

FIG. 2. (a) Fabrication of multiple $SrRuO_3$ devices of grown on Nb:STO. Analyses were done on many different devices to understand the electronic behavior of the film-substrate interface. (b) Schematic diagram of BEEM, where the Pt-Ir STM tip injects hot electrons over the vacuum barrier into a thin metallic film of $SrRuO_3$. The transmitted electrons that satisfy the energy and momentum criteria to overcome the SBH at the interface are collected in the Nb:STO semiconductor.

schematics of BEEM is shown in Fig. 2(b). In our studies, the BEEM current (I_B) is recorded at different local regions of the device. The BEEM transmission depends exponentially on the thickness of the $SrRuO_3$ (d_{SrRuO_3}) film and can be expressed as[11,38] :

$$\frac{I_B}{I_T} = C(E) \times exp\left[-\frac{d_{SrRuO_3}}{\lambda_{SrRuO_3}(E)}\right] \quad (1)$$

where λ_{SrRuO_3} is the hot electron attenuation length, I_T is the tunnel current and $C(E)$ is a constant. In accordance to the Bell-Kaiser model, the local SBH at the $SrRuO_3$/Nb:STO interface is given by[34,35]:

$$\sqrt{\frac{I_B}{I_T}} \propto (V_T - \phi) \quad (2)$$

III. RESULTS AND DISCUSSION

Figure 3(a) shows the STM topography image of the top surface of $SrRuO_3$ deposited on T-Nb:STO. Clear trenches are observed for local SrO terminations in T-NbSTO with an average width between 30-40 nm. As the technique of BEEM is spatially resolved, we can record a large number of BEEM spectra both inside and outside the trenches. BEEM transmission was recorded for many such trenches across several devices. The representative average BEEM spectra across SrO termination in T-Nb:STO is shown in Fig. 3(b). We observe no transmission until a threshold value of the tip bias, which corresponds to the local SBH, as derived from the Bell-Kaiser (B-K) theory from Eq. 2. As observed from Fig. 3(b), the local SBH extracted is 1.28±0.03 eV. For the same device, regions where $SrRuO_3$ grew on TiO_2 terminations (i.e. on terraces) were also probed and their representative BEEM spectra and corresponding local SBH is shown in Fig. 3(c). Thus, with a local SBH difference of 0.20 eV, a clear difference in the interfacial potential landscapes for $SrRuO_3$ on local SrO and TiO_2 terminations of the substrate is observed.

As the local SrO terminated regions in T-Nb:STO are mostly confined to the terrace edges and occur in small pockets, it is not apparently clear whether the growth of $SrRuO_3$ in such confined regions could alter the electronic property at the interface by possible occurrences of defects and changes in local strain. In order to rule out

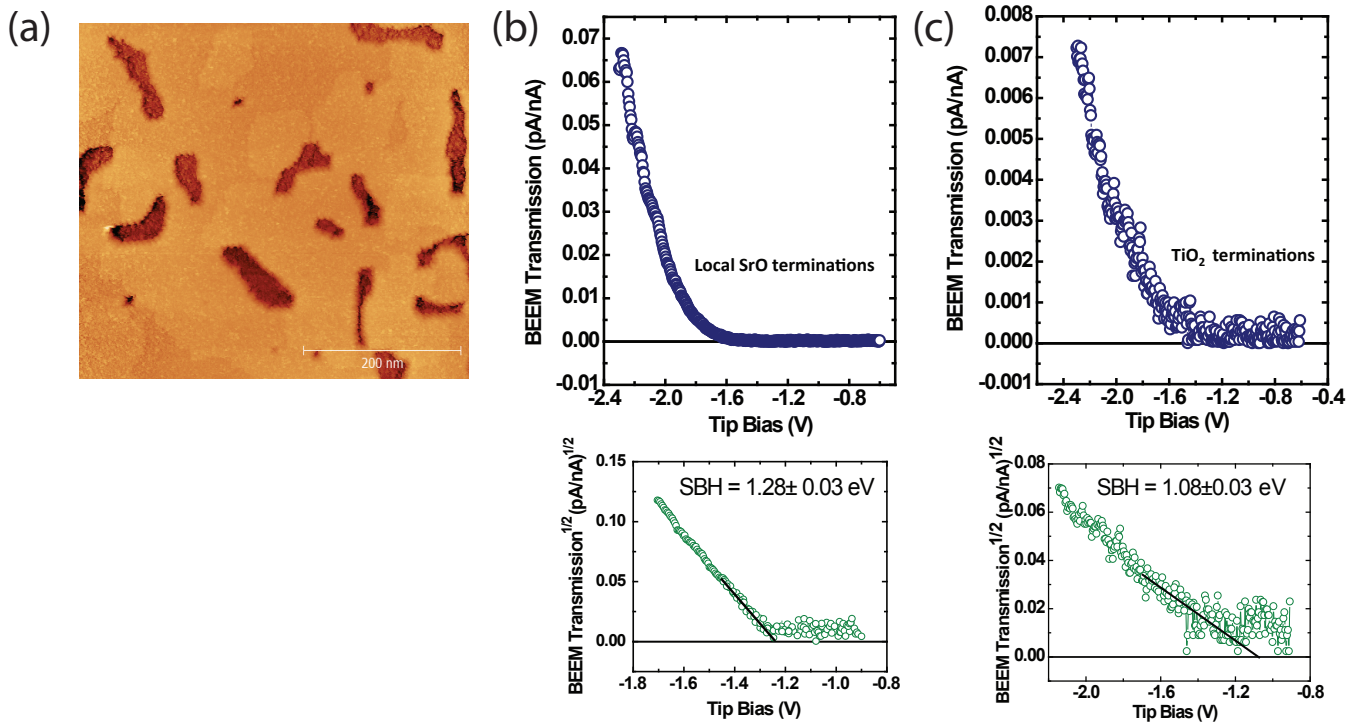

FIG. 3. (a) STM topography of 8 u.c. of $SrRuO_3$ grown on T-Nb:STO at V_{tip} = -1.4 V and I_{tunnel} = 4 nA. Occasional dark patches indicate thinner $SrRuO_3$ grown on SrO terminations of the substrate. (b) Corresponding BEEM spectra for tip placed in dark patches (trenches) i.e. on SrO terminations of the substrate. The extracted corresponding local SBH is represented below. (c) BEEM spectra for tip placed on TiO_2 terminated regions, i.e. on thicker $SrRuO_3$ growth. Corresponding local Schottky barrier height below.

any such contributions to the band alignment at the interface, we engineer the substrate terminating layer as is done in S-Nb:STO. We study electronic transport across it using BEEM and compare the extracted local SBH with that obtained for $SrRuO_3$ grown inside the trenches of T-Nb:STO. Figure 4(a) shows the STM topography image of the top surface of SRO grown on S-Nb:STO. By locating the tip on the flat regions of the terraces, several BEEM spectra were obtained and an average of such spectra taken on several such regions is shown in Fig. 4(b). By fitting the B-K model, we extract the local SBH (Fig. 4(c)). Our findings highlight the following key features:

1. A comparison of the BEEM transmission at SrO terminations in Fig. 3(b) and 4(b) shows that it is higher in T-Nb:STO than in S-Nb:STO. This deviation, of an order of magnitude, is a result of the variation in thickness of $SrRuO_3$ on SrO terminations on either substrates. The growth rate in local SrO terminated pockets is lower than on the terraces of T-Nb:STO, and thus the thickness of $SrRuO_3$ grown inside the trenches are less than 8 u.c. However for S-Nb:STO, an uniform 8 u.c. of $SrRuO_3$ is grown on the engineered interface which is thicker than the above and thus results in a lower BEEM transmission in this case.

2. The local SBHs extracted from the different SrO terminations for both devices (T-Nb:STO and S-Nb:STO) yield the same value of 1.28±0.03 eV.

It is fascinating to find that such a deliberate design of the oxide interface by merely changing the substrate termination can influence the electronic transport across such ionic interfaces. Further, this measurement confirms that the different energy band line-ups at the M-S interface is truly governed by the terminating layer of the substrate; which is primarily caused by changes in the interface dipoles and is thus an intrinsic property of the interface itself.

To understand the intrinsic origin of the differences in the electronic structure of S-Nb:STO and T-Nb:STO, we propose the creation of an interfacial dipole that is different at both the interfaces, thus bringing in a change in the SBH. However, the occurrence of such an induced dipole is puzzling at the symmetric $SrRuO_3$/Nb:$SrTiO_3$ interface. One possible reason for this could be due to a small amount of intermixing of the adjoining Ru/Ti sites. This can be triggered by the different surface energies of the terminating planes of SrO and TiO_2 at the surface of Nb:$SrTiO_3$[39]. This can result in an intermixing of Ru/Ti ions of S-Nb:STO due to the close matching of the ionic radii of Ru^{4+} and Ti^{4+} (Ru^{4+} =

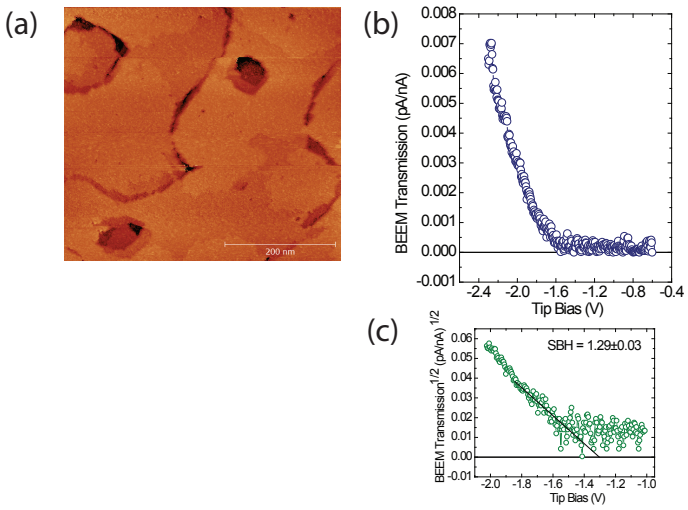

FIG. 4. (a) STM topography of 8 u.c. of $SrRuO_3$ grown on S-Nb:STO at V_{tip} = -1.4 V and I_{tunnel} = 4 nA. (b) Corresponding BEEM spectra through 8 u.c. of $SrRuO_3$ grown on S-Nb:STO. (c) The extracted local Schottky barrier height. Clearly, the local SBH matches with that extracted from $SrRuO_3$ grown inside the trenches of T-Nb:STO as shown in Fig. 3(b).

76 pm and Ti^{4+} = 74 pm); hence lowering the surface energy of the S-Nb:STO interface.

Considering such a scenario, first principles DFT calculations were performed using the QuantumESPRESSO package[40] using the Perdew-Burke-Ernzerhof generalized gradient approximation (GGA) functional[41]. The interface for T-Nb:STO is considered pristine and the S-Nb:STO interface is simulated by a 50% intermixing of Ru and Ti ions. The supercells are constructed by stacking the structural unit cells of $SrRuO_3$ and $SrTiO_3$ along the [001] direction (z direction). Both supercells are fully atomically relaxed until forces are less than 20 meV/Å with the constraint that the in-plane lattice constant of the supercell has the GGA calculated lattice constant of cubic $SrTiO_3$, a=3.937Å. This was done to simulate epitaxial growth of $SrRuO_3$ on a $SrTiO_3$ substrate. Results of the relaxation for both cases are shown in Fig. 5(a-b). For the interface at T-Nb:STO, only a small out-of-plane metal/oxygen displacement is present, indicating that the structure is close to the natural continuation of both perovskite structures at the interface. For the S-Nb:STO intermixed interface, however, large displacement of the Sr sites with respect to oxygen sites is readily apparent. The large difference in displacement profile between the two types of interface terminations are expected to lead to a significant difference in the electrostatic interface dipole between $SrRuO_3$ and $SrTiO_3$, and should therefore be apparent in the electronic band line-up. Indeed, this is the case as can be seen in the local density of states (LDOS) deep inside the $SrTiO_3$ as shown in Fig. 5(c). It is observed that the variation of the interface composition leads to a linear change of the $SrTiO_3$ conduction band offset with respect to the T-Nb:STO and hence to a linear change of the Schottky barrier height at this interface. Indeed we see that the S-Nb:STO interface has an n-type SBH 0.19 eV larger than the T-Nb:STO interface. This is remarkably similar to the experimentally measured difference in n-SBH between the S-Nb:STO and T-Nb:STO.

IV. CONCLUSIONS

The main result of this research is the effect of engineering the termination of the substrate on electronic transport at the film/substrate interface. We investigate this using a vertical device scheme of $SrRuO_3$ on Nb:STO and engineer the Nb:STO interface by inserting a monolayer of SrO. Local differences in the SBH at the interface between engineered/non-engineered is 0.19 eV, thereby indicating different energy band line-ups. At the engineered interface, the differences in the spacing between the atomic planes lead to the creation of an interfacial dipole that is different from that of the non-engineered interface. Our DFT calculations simulated cation intermixing as the probable cause for the interface asymmetry, which matches closely to our experimental results. While intermixing at the interface successfully explains the difference in band-alignments for the two devices, a different amount of oxygen vacancies at the S-Nb:STO and T-Nb:STO interfaces could also play an important role in the interfacial structural distortion[42]. The presence of oxygen vacancy in the SrO plane significantly reduces the electron repulsion in that direction (c-axis) and that results in an increased displacement between the atomic planes at the interface. This also impacts Ti-O-Ru bond angle thereby altering the local electrostatic potential at the $SrRuO_3$/S-Nb:STO interface. Our study emphasizes the flexibility that substrate termination offers in the designing of electronic interfaces for diverse applications in oxide electronics.

We thank B. Noheda and T. T. M. Palstra for use of the Pulsed Laser Deposition system. Technical support from J. Baas and J. G. Holstein is thankfully acknowledged. This work is supported by the Netherlands Organization for Scientific Research NWO-FOM (nano) and the Rosalind Franklin Fellowship program. The research work at the University of Nebraska-Lincoln was supported by the National Science Foundation (NSF) through the Nebraska Materials Research Science and Engineering Center (MRSEC) (NSF grant No. DMR-1420645) and the Nanoelectronics Research Initiative (NRI) through the Center for Nanoferroic Devices (CNFD).

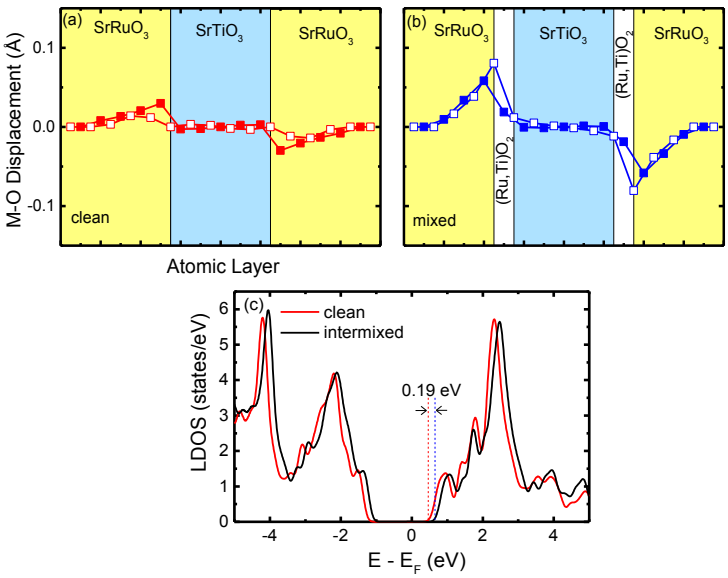

FIG. 5. Layer-by-layer metal-oxygen displacements for the two $SrRuO_3/SrTiO_3$ supercells used to simulate the (a) T-Nb:STO and (b) S-Nb:STO interface. Solid symbols indicate the (Ru or Ti)O_2 displacements and the open symbols are for the SrO layers. (c) The local density of states (LDOS) in the center of the $SrTiO_3$ for both interface terminations. Vertical dashed lines indicate the position of the conduction band minimum (CBM) with respect to the Fermi level, E_F.

* corresponding author; t.banerjee@rug.nl

[1] A. Ohtomo, H. Y. Hwang, *Nature* **427**, 423 (2004).
[2] A. Brinkman, M. Huijben, M. van Zalk, J. Huijben, U. Zeitler, J. C. Maan, W. G. van der Wiel, G. Rijnders, D. H. A. Blank, H. Hilgenkamp, *Nat. Mater.* **6**, 493 (2007).
[3] S. Thiel, G. Hammerl, A. Schmehl, C. W. Schneider, J. Mannhart, *Science* **313**, 1942 (2006).
[4] E. Y. Tsymbal, E. R. A. Dagotto, C. B. Eom, and R. Ramesh, Eds. *Multifunctional Oxide Heterostructures* (Oxford University Press, 2012), p 416.
[5] D. H. Lowndes , D. B. Geohegan, A. A. Puretzky, D. P. Norton, C. M. Rouleau, *Science* **273**, 898 (1996).
[6] H. N. Lee, H. M. Christen, M. F. Chisholm, C. M. Rouleau, D. H. Lowndes, *Nature* **433**, 395 (2005).
[7] D. G. Schlom, J. H. Haeni, J. Lettieri, C. D. Theis, W. Tian, J. C. Jiang, X. Q. Pan, *Mater. Sci. Eng. B* **87**,282 (2001).
[8] M. P. Warusawithana, E. V. Colla, J. N. Eckstein, M. B. Weissman, *Phys. Rev. Lett.* **90**, 036802 (2003).
[9] M. Varela, S. D. Findlay, A. R. Lupini, H. M. Christen, A. Y. Borisevich, N. Dellby, O. L. Krivanek, P. D. Nellist, M. P. Oxley, L. J. Allen, S. J. Pennycook, *Phys. Rev. Lett.* **92**, 095502 (2004).
[10] M. Minohara, R. Yasuhara, H. Kumigashira, M. Oshima, *Phys. Rev. B* **81**, 235322 (2010).
[11] K. G. Rana, T. Yajima, S. Parui, A. F. Kemper, T. P. Devereaux, Y. Hikita, H. Y. Hwang, T. Banerjee, *Sci. Rep.* **3**, 1274 (2013).
[12] K. G. Rana, S. Parui, T. Banerjee, *Phys. Rev. B* **87**, 085116 (2013).
[13] A. M. Kamerbeek, P. Högl, J. Fabian, T. Banerjee, *Phys. Rev. Lett.* **115**, 136601 (2015).
[14] A. Ohtomo, D. A. Muller, J. L. Grazul, H. Y. Hwang, *Nature* **419**, 387 (2002).
[15] S. Okamoto, A. J. Millis, *Nature* **428**, 630 (2004).
[16] N. Nakagawa, H. Y. Hwang, D. A. Muller, *Nat. Mater.* **5**, 204 (2004).
[17] N. Reyren, S. Thiel, A. D. Caviglia, L. Fitting Kourkoutis, G. Hammerl, C. Richter, C. W. Schneider, T. Kopp, A. S. Retschi, D. Jaccard, M. Gabay, D. A. Muller, J.-M. Triscone, J. Mannhart, *Science* **317**, 1196 (2007).
[18] A. D. Caviglia, S. Gariglio, N. Reyren, D. Jaccard, T. Schneider, M. Gabay, S. Thiel, G. Hammerl, J. Mannhart, J.-M. Triscone, *Nature* **456**, 624 (2008).
[19] Guneeta Singh-Bhalla, C. Bell, J. Ravichandran, W. Siemons, Y. Hikita, S. Salahuddin, A. F. Hebard, H. Y. Hwang, R. Ramesh, *Nat. Phys.* **7**, 80 (2011).
[20] Y. Hotta, T. Susaki, H. Y. Hwang, *Phys. Rev. Lett.* **99**, 236805 (2007).
[21] P. R. Willmott, S. A. Pauli, R. Herger, C. M. Schleptz, D. Martoccia, B. D. Patterson, B. Delley, R. Clarke, D. Kumah, C. Cionca, Y. Yacoby, *Phys. Rev. Lett.* **99**, 155502 (2007).
[22] H. Lu, X. Liu, J. D. Burton, Y. Wang, Y. Zhang, D. J. Kim, A. Stamm, P. Lukashev, C.-W. Bark, D. A. Felker, C. M. Folkman, P. Gao, X. Q. Pan, M. S. Rzchowski, C.-B. Eom, E. Y. Tsymbal, and A. Gruverman, *Adv. Mater.* **24**, 1209 (2012).
[23] D. Lee, H. Lu, Y. Gu, S.-Y. Choi, S. Li, S. Ryu, T. R. Paudel, K. Song, E. Mikheev, S. Lee, S. Stemmer, D. A. Tenne, S. H. Oh, E. Y. Tsymbal, X. Wu, L.-Q. Chen, A. Gruverman, and C. B. Eom, *Science* **349**, 1314 (2015).
[24] J. D. Burton and E. Y. Tsymbal, *Phys. Rev B* **82**, 161407(R) (2010).
[25] Y. Hikita, Y. Kozuka, T. Susaki, H. Takagi, and H. Y. Hwang, *Appl. Phys. Lett.* **90**, 143507 (2007).

[26] Y. Hikita, M. Nishikawa, T. Yajima, and H. Y. Hwang, *Phys. Rev. B* **79**, 073101 (2009).
[27] T. Yajima, Y. Hikita, M. Minohara, C. Bell, J. A. Mundy, L. F. Kourkoutis, D. A. Muller, H. Kumigashira, M. Oshima, H. Y. Hwang, *Nat. Commun* **6**, 6759 (2015).
[28] S. Roy, C. Autieri, B. Sanyal, T. Banerjee, *Sci. Rep.* **5**, 15747 (2015).
[29] S. Roy, A. M. Kamerbeek, K. G. Rana, S. Parui, T. Banerjee, *Appl. Phys. Lett.* **102**, 192909 (2013).
[30] G. Koster, L. Klein, W. Siemons, G. Rijnders, J. S. Dodge, C. B. Eom, D. H. A. Blank, M. R. Beasley, *Rev. Mod. Phys.* **84**, 253 (2012).
[31] G. Koster, B. L. Kropman, G. J. H. M. Rijnders, D. H. A. Blank, H.Rogalla, *Appl. Phys. Lett.* **73**, 2920 (1998).
[32] G. Koster, G. J. H. M. Rijnders, D. H. A. Blank, H.Rogalla, *Appl. Phys. Lett.* **74**, 3729 (1999).
[33] M. Huijben, A. Brinkman, G. Koster, G. Rijnders, H. Hilgenkamp, D. H. A. Blank *Adv. Mater.* **21**, 1665 (2009).
[34] W. J. Kaiser, L. D. Bell, *Phys. Rev. Lett.* **60**, 1406 (1988).
[35] L. D. Bell, W. J. Kaiser, *Phys. Rev. Lett.* **61**, 2368 (1988).
[36] E. Haq, T. Banerjee, M. H. Siekman, J. C. Lodder, R. Jansen, *Appl. Phys. Lett.* **86**, 082502 (2005).
[37] S. Parui, K. G. Rana, L. Bignardi, P. Rudolf, B. J. van Wees, T. Banerjee, *Phys. Rev. B* **85**, 235416 (2012).
[38] M. K. Weilmeier, W. H. Rippard, R. A. Buhrman, *Phys. Rev. B* **59**, R2521 (1999).
[39] R. I. Eglitis, D. Vanderbilt, *Phys. Rev. B* **77**, 195408 (2008).
[40] P. Giannozzi, S. Baroni, N. Bonini, M. Calandra, R. Car, C. Cavazzoni, D. Ceresoli, G. L. Chiarotti, M. Cococcioni, I. Dabo, A. D. Corso, S. d. Gironcoli, S. Fabris, G. Fratesi, R. Gebauer, U. Gerstmann, C. Gougoussis, A. Kokalj, M. Lazzeri, L. Martin-Samos, N. Marzari, F. Mauri, R. Mazzarello, S. Paolini, A. Pasquarello, L. Paulatto, C. Sbraccia, S. Scandolo, G. Sclauzero, A. P. Seitsonen, A. Smogunov, P. Umari, R. M. Wentzcovitch, *J. Phys.: Cond. Mat.* **21**, 395502 (2009).
[41] J. P. Perdew, K. Burke, M. Ernzerhof, *Phys. Rev. Lett.* **77**, 3865 (1996).
[42] W. Sitaputra, N. Sivadas, M. Skowronski, D. Xiao, R. M. Feenstra, *Phys. Rev. B* **91**, 205408 (2015).